Progress In Electromagnetics Research, Vol. 120, 371–385, 2011

FAST ANALYSIS OF ELECTRICALLY LARGE RADOME IN MILLIMETER WAVE BAND WITH FAST MULTIPOLE ACCELERATION

H. F. Meng* **and W. B. Dou**

State Key Laboratory of Millimeter Waves, Southeast University, Nanjing 210096, P. R. China

Abstract—Radome has strong effects on the radiation performances of the antenna in millimeter wave band. In this paper, the aperture integration-surface integration (AI-SI) method is adopted to analyze the electrically large antenna-radome system. The fast multipole method (FMM) is proposed to accelerate the aperture integration and inner surface integration in the AI-SI method. An electrically large antenna-radome system at W band is analyzed and measured. The radiation patterns of the system calculated using the AI-SI method with and without the fast multipole acceleration and the measured patterns are compared. The calculated patterns agree very well with each other, and both have the same agreement with the experimental results. However, the computational time of the proposed analysis with the fast multipole acceleration is reduced significantly.

1. INTRODUCTION

A dielectric radome is placed in front of the antenna to protect the system from various environments. However, the presence of the radome always affects the radiation properties of the enclosed antenna, such as distorting the radiation pattern. Therefore, an accurate analysis of the antenna-radome system is important.

Many methods have been used to analyze the antenna-radome system, such as the full wave method [1–3], the high frequency method [4–7], and the hybrid method [8–10]. As the sizes of the antenna-radome system in millimeter wave band are always electrically large, the efficiency of the full wave methods, such as method of moment (MoM) [1] and the finite element method (FEM) [2], are

Received 11 August 2011, Accepted 21 September 2011, Scheduled 26 September 2011
* Corresponding author: Hongfu Meng (menghongfu@163.com).

very low, even employing the fast algorithm proposed by [11]. In contrast, the high frequency methods, such as the ray tracing method (RT) [4] and the physical optics method (PO) [5–7], have higher efficiency. However, the accuracy of RT is not very high, especially for the radome with small curvature radius. The aperture integration-surface integration (AI-SI) method, which is based on PO, has a good balance between the accuracy and efficiency [6, 7]. It is suitable for the analysis of the electrically large antenna-radome system in millimeter wave band.

In the AI-SI method, the incident fields on the inner surface of the radome have two parts. The first part is determined by integrating the aperture currents over the antenna aperture. Some portion of the first incident fields will transmit through the radome wall and the remaining will be reflected by the wall. The reflected fields have important effects on the flash lobe of the radiation pattern [12–14]. By integrating the reflected fields over the inner surface of the radome, the second incident fields on the inner surface of the radome can be obtained. In the traditional AI-SI method [5–7], the aperture integration of the first incident fields and the inner surface integration of the second incident fields are all determined by direct integration using the Stratton-Chu formulas. As the antenna aperture and the inner surface of the radome are electrically large, these integrations take a lot of time [15].

In MoM, the fast multipole method (FMM) is employed to accelerate the computation of the mutual couplings between different elements [16–19]. The determinations of the aperture integration and inner surface integration in the AI-SI method are similar to the computation of the mutual coupling in MoM. So, in this paper, FMM is proposed to accelerate the above mentioned aperture integration and inner surface integration in the AI-SI method.

Firstly, the general steps of the AI-SI method for the antenna-radome analysis are given. Then, the applications of the fast multipole to accelerate the aperture integration and inner surface integration are presented. Finally, some computational results are compared with the experimental results to show the accuracy and efficiency of the fast multipole accelerated analysis.

2. THE AI-SI METHOD

The AI-SI method is a high-frequency method based on PO. It can analyze the electrically large antenna-radome system very efficiently with acceptable accuracy. It was firstly introduced to analyze the radome by Paris [5], and many other researchers have done a lot of work [6, 7]. The general steps of this method are as follows:

In the antenna-radome model, an aperture antenna in an ideally black screen is enclosed by the dielectric radome [5, 13]. When the equivalent electromagnetic currents on the aperture of the antenna are known, the first incident fields on the inner surface of the radome can be obtained by integrating the currents over the antenna aperture using the following formulas:

$$\begin{aligned}\vec{E}_i(\vec{r}) =& -j\omega\mu \int\limits_{S_{AP}} \left(\bar{\bar{I}} + \frac{\nabla\nabla}{k^2}\right) G(\vec{r},\, \vec{r}\,')\vec{J}_{AP}(\vec{r}\,')dS' \\ & - \nabla \times \int\limits_{S_{AP}} \vec{M}_{AP}(\vec{r}\,')G(\vec{r},\, \vec{r}\,')dS' \\ \vec{H}_i(\vec{r}) =& -j\omega\varepsilon \int\limits_{S_{AP}} \left(\bar{\bar{I}} + \frac{\nabla\nabla}{k^2}\right) G(\vec{r},\, \vec{r}\,')\vec{M}_{AP}(\vec{r}\,')dS' \\ & + \nabla \times \int\limits_{S_{AP}} \vec{J}_{AP}(\vec{r}\,')G(\vec{r},\, \vec{r}\,')dS'\end{aligned} \tag{1}$$

where

$$G\left(\vec{r},\, \vec{r}\,'\right) = \frac{e^{-jk|\vec{r}-\vec{r}\,'|}}{4\pi\left|\vec{r}-\vec{r}\,'\right|} \tag{2}$$

is the Green's function in free space, $\vec{J}_{AP}$, $\vec{M}_{AP}$ are the electromagnetic currents on the antenna aperture, and S_{AP} is the antenna aperture.

The incident vector at the intersection point on the inner surface of the radome is established by the direction of the Poynting vector [5]

$$\hat{S}_i = \mathrm{Re}\left(\vec{E}_i \times \vec{H}_i^*\right) / \left|\mathrm{Re}\left(\vec{E}_i \times \vec{H}_i^*\right)\right| \tag{3}$$

The incident vector and the normal vector at the intersection point on the inner surface define the plane of incidence. The incident fields at the intersection point are decomposed into the perpendicular and parallel polarization components to the plane of incidence. After reflection and refraction by the radome wall, the reflected fields $\vec{E}_r$, $\vec{H}_r$ on the inner surface and the transmitted fields $\vec{E}_t$, $\vec{H}_t$ on the outer surface of the radome are recombined as [7]

$$\begin{aligned}\vec{E}_r &= \left(\vec{E}_i \cdot \vec{v}_\perp^{\,i}\right) R_\perp \vec{v}_\perp^{\,r} + \left(\vec{E}_i \cdot \vec{v}_{//}^{\,i}\right) R_{//} \vec{v}_{//}^{\,r} \\ \vec{H}_r &= \left(\vec{H}_i \cdot \vec{v}_\perp^{\,i}\right) R_{//} \vec{v}_\perp^{\,r} + \left(\vec{H}_i \cdot \vec{v}_{//}^{\,i}\right) R_\perp \vec{v}_{//}^{\,r}\end{aligned} \tag{4}$$

$$\begin{aligned}\vec{E}_t &= \left(\vec{E}_i \cdot \vec{v}_\perp^{\,i}\right) T_\perp \vec{v}_\perp^{\,t} + \left(\vec{E}_i \cdot \vec{v}_{//}^{\,i}\right) T_{//} \vec{v}_{//}^{\,t} \\ \vec{H}_t &= \left(\vec{H}_i \cdot \vec{v}_\perp^{\,i}\right) T_{//} \vec{v}_\perp^{\,t} + \left(\vec{H}_i \cdot \vec{v}_{//}^{\,i}\right) T_\perp \vec{v}_{//}^{\,t}\end{aligned} \tag{5}$$

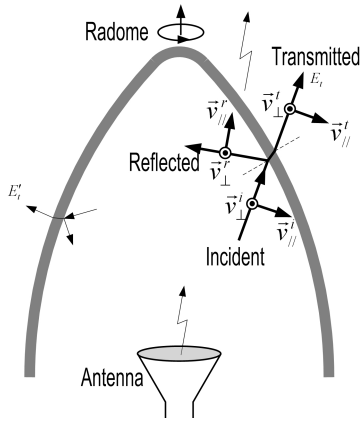

Figure 1. Model of the AI-SI method for the antenna-radome analysis.

where $\vec{v}_{\perp}$ and $\vec{v}_{//}$ are the unit vectors illustrated in Figure 1, the superscripts i, r, and t represent the incident, reflected, and transmitted fields, respectively. $R_{\perp}$, $R_{//}$, $T_{\perp}$, $T_{//}$ are the reflection and transmission coefficients for the perpendicular and parallel polarization components [7, 20].

The reflected fields on the inner surface may bounce in the radome and they have important effects on the flash lobe of the antenna-radome system [12–14]. In order to account the mutual interactions between different parts of the radome, the fields radiated from the reflected fields must be calculated. So, the equivalent reflected currents on the inner surface of the radome are

$$\vec{J}_r = \hat{n} \times \vec{H}_r \quad \vec{M}_r = -\hat{n} \times \vec{E}_r \tag{6}$$

where $\hat{n}$ is the normal vector on the inner surface of the radome.

As the flange of the aperture antenna is modeled as black screen, the fields reflected to the bottom of the radome are ignored. However, the fields reflected to the inner surface of the radome may form second radiation. Thus, the second incident fields on the inner surface of the radome can be determined as follows:

$$\begin{aligned} \vec{E}'_i(\vec{r}) \;=\; & -j\omega\mu \int\limits_{S_{Rin}} \left(\bar{\bar{I}} + \frac{\nabla\nabla}{k^2} \right) G\left(\vec{r},\, \vec{r}\,'\right) \vec{J}_r(\vec{r}\,')dS' \\ & -\nabla \times \int\limits_{S_{Rin}} \vec{M}_r(\vec{r}\,')G\left(\vec{r},\, \vec{r}\,'\right) dS' \end{aligned}$$

$$\vec{H}'_i(\vec{r}) = -j\omega\varepsilon \int\limits_{S_{Rin}} \left(\bar{\bar{I}} + \frac{\nabla\nabla}{k^2}\right) G\left(\vec{r}, \vec{r}'\right) \vec{M}_r(\vec{r}')dS' + \nabla \times \int\limits_{S_{Rin}} \vec{J}_r(\vec{r}')G\left(\vec{r}, \vec{r}'\right) dS' \quad (7)$$

where $G(\vec{r}, \vec{r}')$ is the Green's function in free space defined in (2) and S_{Rin} is the inner surface of the radome.

The second incident fields are treated the same as the first incident fields in (5) and the second transmitted fields $\vec{E}'_t$, $\vec{H}'_t$ can be obtained.

Finally, the total fields on the outer surface of the radome are the vector sum of the first and second transmitted fields:

$$\vec{E}_t^{total} = \vec{E}_t + \vec{E}'_t \quad \vec{H}_t^{total} = \vec{H}_t + \vec{H}'_t \quad (8)$$

When the total transmitted fields on the outer surface are known, the far field radiation patterns of the antenna-radome system can be determined by integrating the fields over the outer surface of the radome using the Stratton-Chu formulas [6].

3. THE FAST MULTIPOLE ACCELERATION

As above mentioned, the integration (1) needs to be performed over the antenna aperture S_{AP} and the integration (7) needs to be performed over the inner surface of the radome S_{Rin}. In numerical computation, the integration surface S_{AP} and S_{Rin} are meshed into

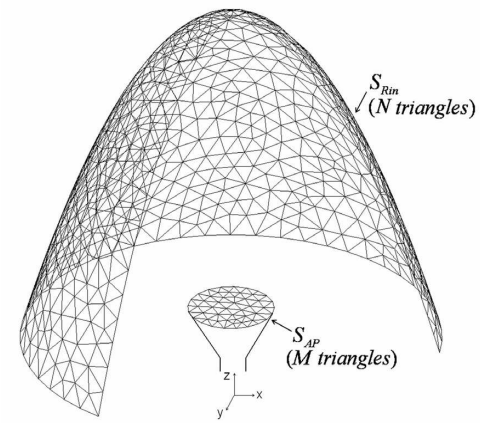

Figure 2. Schematic of the mesh on the antenna aperture and radome surface.

small triangles with the edge length much smaller than the wavelength as in Figure 2, and then the integrations (1) and (7) are converted into the summations over all the triangles. If the antenna aperture S_{AP} is meshed with M triangles and the inner surface of the radome with N triangles, then the computation of the first incident fields on the inner surface of the radome is of $O(MN)$ complexity and the computation of the second incident fields of $O(N^2)$ complexity. As the antenna and radome in millimeter wave band are electrically large and the numbers M and N are large, the aperture integration (1) and inner surface integration (7) demand a long computing time.

In MoM, the impedance matrix shows the mutual coupling between every triangle. FMM is always adopted to accelerate the matrix-vector product [16–19]. FMM was proposed for static problem by Rokhlin in 1987 and for dynamic problems in 1990 [16, 17]. For the matrix-vector product with N unknowns, the two-level FMM reduces both the memory requirement and numerical complexity from $O(N^2)$ to $O(N^{1.5})$ and the three-level FMM reduces it to $O(N^{4/3})$ [16–19]. By using the multilevel fast multipole method (MLFMM), the numerical complexity can be further reduced to $O(N \log N)$ [21–24].

When applying FMM to accelerate the mutual coupling computation, the triangles on the integration surface are divided into groups depending on their position. The key point of FMM is the addition theorem, which is presented as follows:

$$\frac{e^{-jk\left|\vec{R}+\vec{d}\right|}}{\left|\vec{R}+\vec{d}\right|} = -jk\sum_{l=0}^{L}(-1)^l(2l+1)j_l(kd)h_l^{(2)}(kR)P_l(\hat{d}\cdot\hat{R}) \tag{9}$$

where j_l is a spherical Bessel function of the first kind, $h_l^{(2)}$ is a spherical Hankel function of the second kind and P_l is a Legendre polynomial.

The expansion of the product $j_l P_l$ in propagating plane waves is

$$4\pi(-j)^l j_l(kd)P_l\left(\hat{d}\cdot\hat{R}\right) = \iint_{4\pi} e^{-jk\hat{k}\cdot\vec{d}}P_l\left(\hat{k}\cdot\hat{R}\right)d^2\hat{k} \tag{10}$$

Applying the Gaussian-Legendre quadrature to (10) and substituting (9) and (10) into (2), the Green's function can be expressed as

$$G\left(\vec{r},\vec{r}\,'\right) = \frac{e^{-jk\left|\vec{R}+\vec{d}\right|}}{4\pi\left|\vec{R}+\vec{d}\right|} = \frac{-jk}{(4\pi)^2}\sum_{p=1}^{K}\left[\omega_p e^{-j\vec{k}_p\cdot\vec{d}}\sum_{l}^{L}(-j)^l(2l+1)h_l^{(2)}(kR)P_l\left(\vec{k}_p\cdot\hat{R}\right)\right] \tag{11}$$

where $\vec{R}$ is the vector from the source group center to the field group center, $\vec{d}$ is the summation of the vectors from the source point to source group center and from the field group center to field point, R and d are their amplitudes with $R > d$, and $\hat{R}$ and $\hat{d}$ are the unit vectors, respectively.

In (9), L is an infinite number. However, in numerical practice, L must be truncated with the finite number of modes and the relative error is depending on L with the following relationship [18, 21]:

$$L = kd_{\max} + \gamma \ln(\pi + kd_{\max}) \tag{12}$$

where $d_{\max}$ is the maximal diameter of all the groups. The relative error of (11) can less than 0.1 when $\gamma = 1$ and the larger of γ, the more accurate of (11).

In (11), K is the number of integration points over the unit sphere and is always chosen as

$$K = 2L^2 \tag{13}$$

When $kR > L$, the source group and field group are called far groups. The interactions between the triangles in the far groups in the integrals (1) and (7) can be calculated as follows: the fields from all the triangles in the source group are aggregated to the source group center firstly, then, the field information is transformed from the source group center to the field group center, and finally, the field effect is disaggregated to every triangle in the field group.

The integration formula between the far groups can be replaced by:

$$\begin{aligned}\vec{E}^{far}(\vec{r}) = & -j\omega\mu \int_S \frac{-jk}{(4\pi)^2} \sum_{p=1}^{K} \left(\bar{\bar{I}} - \hat{k}\hat{k}\right) \\ & \left[\omega_p e^{-j\vec{k}_p \cdot \vec{d}} \sum_{l}^{L} (-j)^l (2l+1) h_l^{(2)}(kR) P_l\left(\vec{k}_p \cdot \hat{R}\right) \vec{J}(\vec{r}')\right] \\ & -(-jk) \int_S \frac{-jk}{(4\pi)^2} \sum_{p=1}^{K} \hat{k} \\ & \times \left[\omega_p e^{-j\vec{k}_p \cdot \vec{d}} \sum_{l}^{L} (-j)^l (2l+1) h_l^{(2)}(kR) P_l\left(\vec{k}_p \cdot \hat{R}\right) \vec{M}(\vec{r}')\right] \end{aligned} \tag{14}$$

When kR is comparable or smaller than L, the source and field group are near groups. At this time, the Equation (11) can not get desired accuracy and the effects between the triangles in the near groups must be calculated using the traditional direct integration.

Finally, the integrals (1) and (7) can be expressed as

$$\vec{E}(\vec{r}) = \vec{E}^{near}(\vec{r}) + \vec{E}^{far}(\vec{r}) \tag{15}$$

in which $\vec{E}^{near}(\vec{r})$ is calculated with the traditional direct integration in the near group triangles. When applying (14) and (15) to accelerate the aperture integration (1), the symbols $\vec{E}(\vec{r})$, $\vec{J}(\vec{r}')$ and $\vec{M}(\vec{r}')$ represent $\vec{E}_i(\vec{r})$, $\vec{J}_{AP}(\vec{r}')$ and $\vec{M}_{AP}(\vec{r}')$, and when applying them to (7), they are $\vec{E}'_i(\vec{r})$, $\vec{J}_r(\vec{r}')$ and $\vec{M}_r(\vec{r}')$, respectively.

For the aperture integration (1), the integration only needs to calculate the mutual interactions from the aperture triangles to triangles on the inner surface of the radome. As the radome is several wavelengths away from the antenna as shown in Figure 3, all the groups between the aperture and the radome are far groups, then the fast multipole acceleration will be very significant.

For the inner surface integration of (7), the schematic of the application of the fast multipole acceleration is shown in Figure 4. As the distances between most groups are larger than L, FMM will reduce the computing time between the far groups very significantly. However, in the top of the radome, where the distances between the groups are comparable with the group size, FMM will not be used.

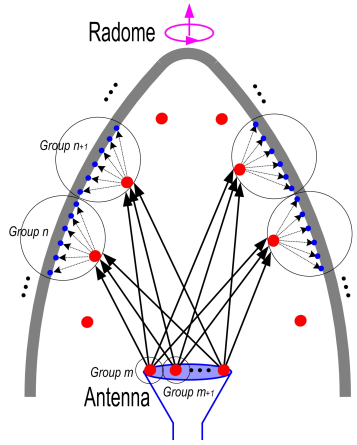

Figure 3. Schematic of the application of FMM to accelerate the aperture integration.

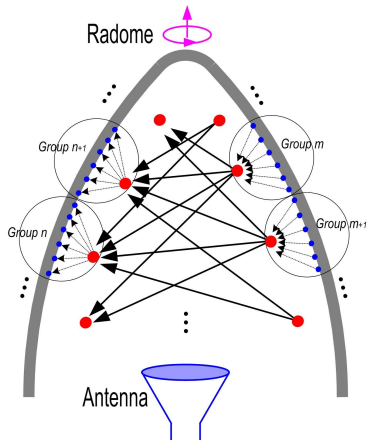

Figure 4. Schematic of the application of FMM to accelerate the inner surface integration.

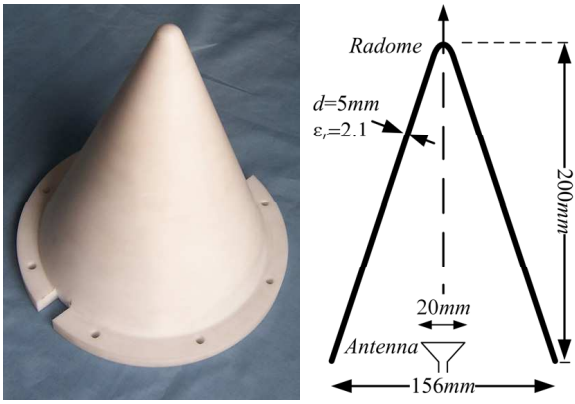

Figure 5. The photo and geometrical sizes of the millimeter wave radome.

4. RESULTS

To confirm the validity and efficiency of the fast multipole acceleration, an electrically large antenna-radome system at W band are fabricated and measured. The radiation patterns of the antenna-radome system determined by the AI-SI method with the fast multipole acceleration are compared with the calculated and measured results in the pervious work [7].

The photo and geometrical sizes of the millimeter wave radome are shown in Figure 5. The radome has a height of 200 mm and a base diameter of 156 mm. In the front of the radome, there is an arc with the curvature radius of 8 mm. The radome is made of Teflon with the relative permittivity of 2.1 and the thickness is 5 mm. A conical horn with the aperture diameter of 20 mm is enclosed by the radome. The horn can rotate around the gimbal center, which is located at the base center of the radome. The antenna-radome system is operating at 94 GHz.

Firstly, the first incident fields on the radome are calculated by direct integration using (1) and by integration with the fast multipole acceleration using (14) and (15). In FMM, the triangles on the aperture and radome are divided into groups with the maximal diameter $d_{\max} = 1.25\lambda$. In order to obtain enough accuracy, the parameters in (12) are chosen as $\gamma = 1$ and $L = 10$, thus the relative error of FMM result can be less than 0.1. The Gauss-Legendre integration number is $K = 2L^2 = 200$. The distributions of the electrical field components E_y and E_z on the inner surface of the radome are compared in Figure 6.

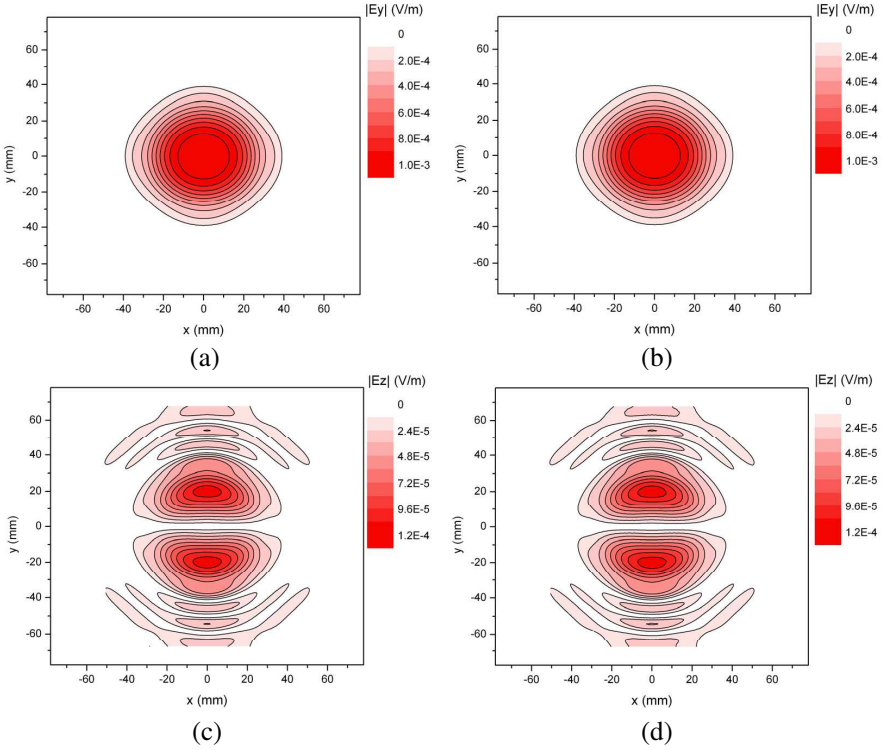

Figure 6. The distributions of the electrical field components on the inner surface of the radome, (a) E_y computed by direct integration, (b) E_y computed by integration with the fast multipole acceleration, (c) E_z computed by direct integration, (d) E_z computed by integration with the fast multipole acceleration.

As the conical horn is linear polarized in y direction, the electrical field component E_x is very small and is not given here. It is clear that the electrical field distributions calculated by direct integration and by fast multipole accelerated integration have good agreement with each other.

Then, the radiation patterns of the antenna-radome system are computed. In order to shown the accuracy of FMM, the radiation patterns determined by FMM with different the number of modes ($L = 8$, 10 and 12) are compared with the direct integration result in Figure 7. It is clear that, the result of $L = 8$ has obvious differences with the direct integration result, however, the results of $L = 10$ and 12 agree very well with it. As discussed in (12), when $L = 8$, the

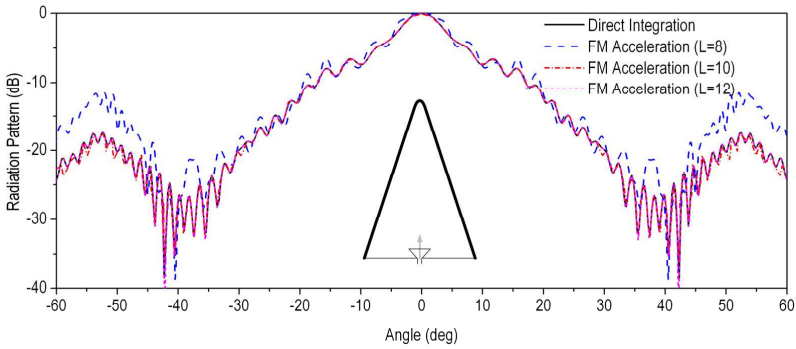

Figure 7. Calculated H plane radiation patterns using AI-SI with fast multipole acceleration compares with the result in [7] calculated by direct integration.

relative error of (11) will be very significant. However, when $L = 10$, it will be less than 0.1, and 0.01 for $L = 12$. The results agree with the conclusion in [21] as compared in Figure 7.

For this antenna-radome system at W band, the direct integration of AI-SI needs about 1 h to calculate the aperture integration and 19 h for the inner surface integration. However, by applying the fast multipole acceleration with $L = 10$, it takes only 12 m for the aperture integration and 6 h for inner surface integration. The fast multipole acceleration reduces the computational time of the antenna-radome analysis significantly, especially the time for the aperture integration. When the number of modes L in FMM becomes large, the computational time will increase quickly, for example, 28 m for the aperture integration and 13 h for the inner surface integration with $L = 12$. However, as in Figure 7, the accuracy is improved a little. In the following antenna-radome analysis, the number of modes is $L = 10$.

The calculated radiation patterns of the antenna-radome system using the fast multipole accelerated AI-SI with the number of modes $L = 10$ are compared with the measured radiation patterns in Figure 8. It can be seen that the results with fast multipole acceleration have some agreements with the measured patterns. They have the same accuracy with the direct integration method as in [7].

Finally, the antenna tilts 10° in the H plane as in [7]. The calculated radiation pattern with the fast multipole acceleration and the results in [7] are illustrated in Figure 9. The radiation patterns calculated with and without FMM acceleration agree very well with each other and they both have the same agreement with the measured result.

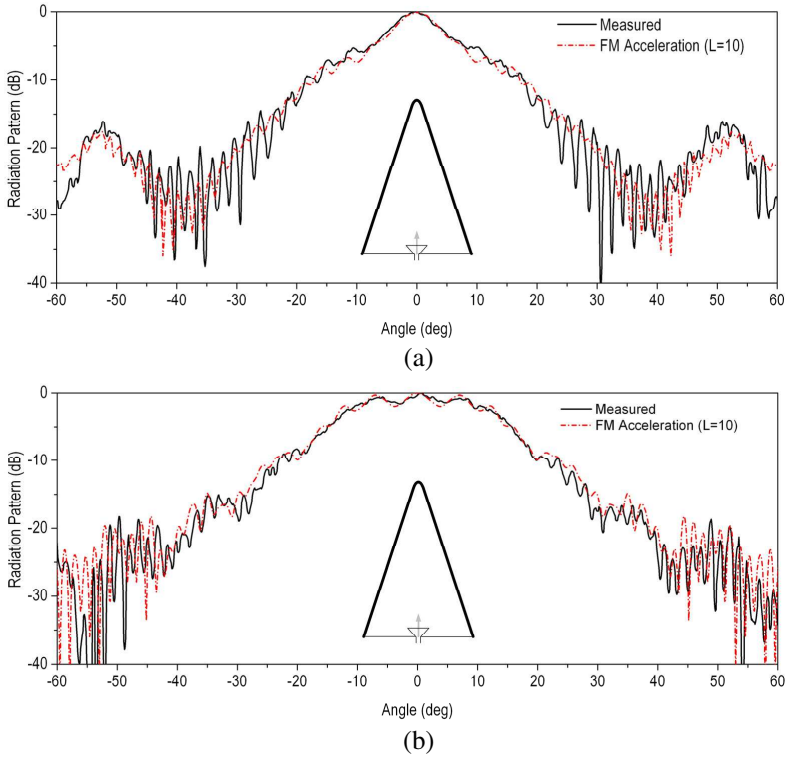

Figure 8. Measured and calculated radiation patterns of the conical radome enclosed conical horn, (a) H plane, (b) E plane.

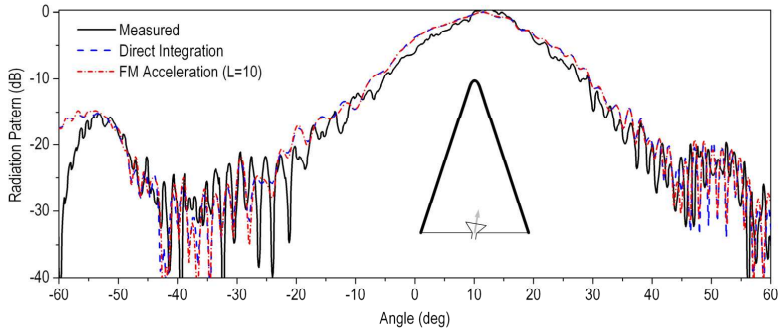

Figure 9. Measured and calculated H plane radiation patterns of the conical radome enclosed conical horn when the horn tilts 10° in H plane.

Up to now, the full wave methods (MLFMM, MoM and FEM) have high accuracy for antenna-radome analysis, but their only suitable for electrically small system. The RT method has higher efficiency and lower accuracy. However, the proposed FMM accelerated AI-SI reduces the computational complexity of PO based method significantly and keeps an acceptable accuracy. It is more accuracy and more efficiency than the other methods for the analysis of electrically large radome in millimeter wave band.

5. CONCLUSION

In this paper, an electrically large antenna-radome system in millimeter wave band is analyzed using the AI-SI method. The fast multipole method is adopted to accelerate the aperture integration from the antenna to the radome and the surface integration on the inner surface of the radome. The calculated radiation patterns have good agreements with the experimental results and direct integration results. The efficiency of the present method is much higher than the traditional direct integration method and the accuracies of the two methods are comparable. It is suitable for fast analysis of the antenna-radome system in millimeter wave band.

ACKNOWLEDGMENT

This work is supported by the National Natural Science Foundation of China under grant 60571028 and the State Key Laboratory of Millimeter Waves under grant Z200920.

REFERENCES

1. Arvas, E., A. Rahhalarabi, U. Pekel, et al., "Electromagnetic transmission through a small radome of arbitrary shape," *IEE Proceedings-H Microwaves, Antennas and Propagation*, Vol. 137, No. 6, 401–405, 1990.
2. Povinelli, M. J. and J. D'Angelo, "Finite element analysis of large wavelength antenna radome problems for leading edge and radar phased arrays," *IEEE Transactions on Magnetics*, Vol. 27, No. 5, 4299–4302, 1991.
3. Nie, X.-C., N. Yuan, L.-W. Li, T. S. Yeo, and Y.-B. Gan, "Fast analysis of electromagnetic transmission through arbitrary shaped airborne radomes using precorrected-FFT method," *Progress In Electromagnetics Research*, Vol. 54, 37–59, 2005.

4. Lee, H.-S. and H. Park, "Prediction of radome bore-sight errors using a projected image of source distributions," *Progress In Electromagnetics Research*, Vol. 92, 181–194, 2009.
5. Paris, D., "Computer-aided radome analysis," *IEEE Trans. Antennas Propag.*, Vol. 18, No. 1, 7–15, 1970.
6. Kozakoff, D. J., *Analysis of Radome-enclosed Antennas*, Artech House, Boston, London, 1997.
7. Meng, H.-F., W.-B. Dou, T.-T. Chen, et al., "Analysis of radome using aperture integration-surface integration method with modified transmission coefficient," *Journal of Infrared, Millimeter, and Terahertz Waves*, Vol. 30, No. 2, 199–210, 2009.
8. Hu, B., X.-W. Xu, M. He, and Y. Zheng, "More accurate hybrid PO-MoM analysis for an electrically large antenna-radome structure," *Progress In Electromagnetics Research*, Vol. 92, 255–265, 2009.
9. Meng, H.-F. and W.-B. Dou, "A hybrid method for the analysis of radome-enclosed horn antenna," *Progress In Electromagnetics Research*, Vol. 90, 219–233, 2009.
10. Nie, X.-C., Y.-B. Gan, N. Yuan, C.-F. Wang, and L.-W. Li, "An efficient hybrid method for analysis of slot arrays enclosed by a large radome," *Journal of Electromagnetic Waves Applications*, Vol. 20, No. 2, 249–264, 2006.
11. Lu, C.-C., "A fast algorithm based on volume integral equation for analysis of arbitrarily shaped dielectric radomes," *IEEE Trans. Antennas Propag.*, Vol. 51, No. 3, 606–612, 2003.
12. Oğuzer, T. and A. Altintas, "Analysis of the nonconcentric reflector antenna-in-radome system by the iterative reflector antenna and radome interaction," *Journal of Electromagnetic Waves Applications*, Vol. 21, No. 1, 57–70, 2007.
13. Sukharevsky, I. V., S. E. Vazhinsky, and I. O. Sukharevsky, "3-D radome-enclosed aperture antenna analyses and far-side radiation," *IEEE Trans. Antennas Propag.*, Vol. 58, No. 9, 2843–2849, 2010.
14. Sukharevsky, O. I. and V. A. Vasilets, "Scattering of reflector antenna with conic dielectric radome," *Progress In Electromagnetics Research B*, Vol. 4, 159–169, 2008.
15. Sukharevsky, O. I., V. A. Vasilets, S. V. Kukobko, et al., "The electromagnetic wave scattering by aerial and ground radar objects," Kharkov, Ukraine, KUAF, 2009.
16. Greengard, L. and V. Rokhlin, "A fast algorithm for particle simulation," *J. Comput. Phys.*, Vol. 73, 325–348, 1987.

17. Rokhlin, V., "Rapid solution of integral equations of scattering theory in two dimensions," *J. Comput. Phys.*, Vol. 86, 414–439, Feb. 1990.
18. Coifman, R., V. Rokhlin, and S. Wandzura, "The fast multipole method for the wave equation: A pedestrian prescription," *IEEE Trans. Antennas Propagat. Mag.*, Vol. 35, 7–12, Jun. 1993.
19. Cui, T.-J. and W.-C. Chew, *Fast Algorithms in Computational Electromagnetics*, Artech House, INC, Oct. 2003.
20. Chen, F., Q. Shen, and L. Zhang, "Electromagnetic optimal design and preparation of broadband ceramic radome material with graded porous structure," *Progress In Electromagnetics Research*, Vol. 105, 445–461, 2010.
21. Song, J. M., C. C. Lu, and W. C. Chew, "Multilevel fast multipole algorithm for electromagnetic scattering by large complex objects," *IEEE Trans. Antennas Propag.*, Vol. 45, No. 10, 1488–1493, 1997.
22. Gurel, L., O. Ergul, A. Unal, and T. Malas, "Fast and accurate analysis of large metamaterial structures using the multilevel fast multipole algorithm," *Progress In Electromagnetics Research*, Vol. 95, 179–198, 2009.
23. Eibert, T. F., Ismatullah, E. Kaliyaperumal, and C. H. Schmidt, "Inverse equivalent surface current method with hierarchical higher order basis functions, full probe correction and multi-level fast multipole acceleration," *Progress In Electromagnetics Research*, Vol. 106, 377–394, 2010.
24. Yang, M.-L. and X.-Q. Sheng, "Parallel high-order FE-BI-MLFMA for scattering by large and deep coated cavities loaded with obstacles," *Journal of Electromagnetic Waves and Applications*, Vol. 23, No. 13, 1813–1823, 2009.